

HREM and STEM of defects in multiply-twinned particles

by L. D. MARKS and DAVID J. SMITH*, *Cavendish Laboratory, University of Cambridge, Madingley Road, Cambridge CB3 0HE*, and **High Resolution Electron Microscope, University of Cambridge, Free School Lane, Cambridge CB2 3RQ*

KEY WORDS. HREM, STEM, multiply-twinned particles.

SUMMARY

The structure of defects in multiply-twinned particles has been studied in detail using high-resolution lattice imaging, dark field and microdiffraction techniques. Icosahedral particles with sizes greater than about 15 nm were found to contain defects, in the form of stacking fault loops parallel with the external surface, which were extremely difficult to detect by conventional amplitude contrast techniques. Microdiffraction mappings correlated with these results, showing large rotations of the face-centred cubic segments. Results for decahedral particles indicated the presence of stacking faults running adjacent to, and parallel with, the twin boundaries. Microdiffraction maps confirmed that the particle structure was face-centred cubic, and also verified that the apparent epitaxy of these particles was highly variable. Models for the defects are proposed and discussed, and the relative merits of HREM and STEM for elucidating structural details in small particles is briefly considered. Finally, the potential for direct imaging at surfaces, as demonstrated by some recent images, is discussed.

1. INTRODUCTION

The characterization of metal crystallites in the nanometre-size range is of substantial importance in such diverse fields as thin-film nucleation and growth, heterogeneous catalysis and air pollution. Of particular interest are deviations from 'bulk' behaviour where the treatment of a small particle as a miniature version of a macroscopic single crystal breaks down. It then becomes necessary to take account of the surface of the particles including both physical effects, such as the surface energies and morphologies, as well as any surface diffraction arising from the imaging process. It is the surface which causes the change in internal structure leading to multiply-twinned particles, or MTPs, i.e. the favourable surface energies of certain faces (in particular, 111 faces) promote a particle structure composed of a number of twinned microcrystallites (Marks, 1983).

When considered solely as fcc single crystal aggregates, MTPs are not fully space-filling and some form of internal distortion is required to fill solid angle deficits of approximately 0.08π in decahedral MTPs (Dh) and 0.48π in icosahedral MTPs (Ic). The precise form of these distortions remains a subject of some controversy. In early work (Ino, 1966; Ino & Ogawa, 1967; Allpress & Sanders, 1967; Komoda, 1968) no contrast effects attributable to dislocations were detected in the images and it was assumed that inhomogeneous elastic strains were present. In a later analysis based on high resolution dark field images (Heinemann *et al.*, 1979; Yacaman *et al.*, 1979; Yang, 1979; Yang *et al.*, 1979), it was suggested that homogeneous distortions were present which transformed the Dh's to an orthorhombic crystallography and the Ics to a

rhombic form. Our previous high-resolution lattice imaging observations have shown little obvious evidence for inhomogeneous elastic strains, although demonstrating that small Ics contained a significant number of dislocations (Marks *et al.*, 1980; Smith & Marks, 1981a).

In this paper we report the results of a detailed study of defects and strains in MTPs employing a combination of high resolution lattice imaging and high resolution dark field as well as microdiffraction in a scanning transmission instrument. From the lattice fringe images we have been able to detect evidence for inhomogeneous elastic strains in the region of the surface of the Ics (Section 3.1), as well as details of the defect structure in the two types of MTPs (Sections 3.1 and 3.2). Both the inhomogeneous strains and the dislocations in the Ics produce mainly phase, rather than amplitude, contrast, an effect substantiated by the dark field images, and this explains why earlier lower-resolution work has failed to detect their presence. This interpretation of MTPs as inhomogeneously-strained and dislocated fcc aggregates is also substantiated by the microdiffraction results (Section 3.3). Collation of the experimental evidence allows models for the defects in both types of MTPs to be proposed (Section 4): the relative merits of the various techniques with respect to providing useful structural information is briefly discussed (Section 5).

2. EXPERIMENTAL PROCEDURE

The results presented below were obtained from a number of different samples—we report those generally consistent features which appeared to show little, or no, dependence upon preparation technique or the previous history of the sample.

The stock samples for Ics of gold and silver were prepared by evaporation in a diffusion-pumped system as described elsewhere (Marks & Smith, 1981). Somewhat larger MTPs (25–50 nm in diameter) were observed in a specimen evaporated onto a substrate of KCl, which had been cleaved *in situ* at 300°C in an unbaked, all-metal evaporator. (The primary nuclei in this specimen were (100) epitaxed square pyramids—MTPs were common only as secondary nuclei.) Very large Dh's were found in a silver catalyst sample, details of which have been published elsewhere (Marks & Howie, 1979). A somewhat different type of MTP was observed in a specimen of Au evaporated at room temperature on to *in situ* cleaved KCl in UHV ($< 2 \times 10^{-8}$ Pa). The Dh's in this sample were noticeably rounded (see Figs. 6 and 8), and contained a significantly larger number of defects. However, the actual defect structures appeared to be the same as those observed in particles prepared by other means.

The high resolution lattice images of MTPs were taken with the Cambridge University High Resolution Electron Microscope (HREM) (Smith *et al.*, 1982) operated at either 500 kV or 575 kV. Initially, micrographs from areas of interest were recorded as through focal series (Marks & Smith, 1981) but recent work has been carried out using an image pickup system (Catto *et al.*, 1982). The lattice structure of the particles could then be directly viewed on the television monitor and the required defocus could be chosen with considerable accuracy.

For STEM imaging, and microdiffraction mappings, specimens were examined in a VG-HB5 electron microscope operated at 80 kV. As a compromise between resolution and signal strength, a large objective aperture ($\sim 0.2 \text{ \AA}^{-1}$ radius) and a relatively small collector aperture ($\sim 1\frac{1}{2}$ mrad radius) were normally used, with the condenser lens overexcited to reduce the effects of stray fields in the region of the gun. (The visibility of the 6.8 Å Moiré fringes in MTPs was used as a resolution check.) The microdiffraction maps were collected with a Grigson scanning system, with some low pass filtering to minimize the effects of instrument noise and amorphous carbon speckle structure.

3. EXPERIMENTAL RESULTS

3.1. Icosahedral MTPs

The basic defect structure observed in the icosahedral particles is shown in Fig. 1; namely, a stacking fault which lies parallel with the external surface terminating on a Shockley partial dislocation and extending part-way across one of the (110) oriented segments. The length of the stacking fault and the total number of defects per particle varied somewhat, but a number of

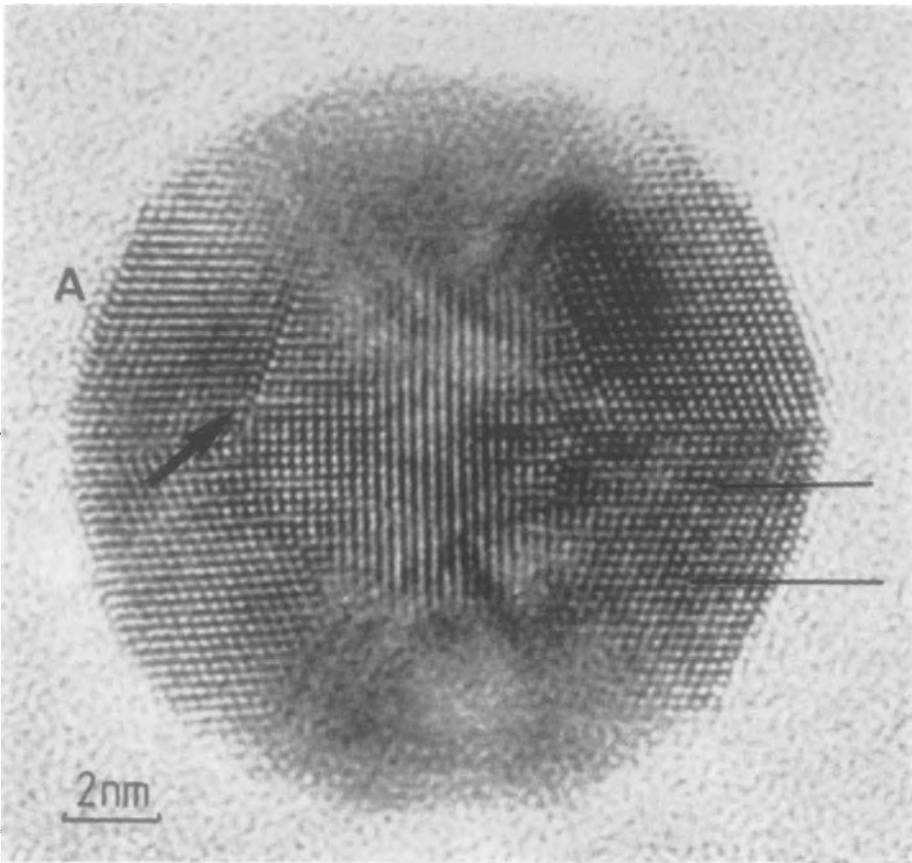


Fig. 1. High resolution lattice image of an Ic showing the basic defect structure. The Shockley partial dislocation and some lattice rotations are indicated. A partial layer where an ordering mistake has occurred can be seen at A.

general characteristics were observed: (1) The defects were present only in particles above about 15 nm in diameter, and showed a noticeable increase both in the number of defects per particle, and the length of the stacking fault, with increasing particle size. An example of a particle containing three dislocations in one segment is shown in Fig. 2. (2) The stacking faults never showed any evidence for reflection across the twin boundaries indicating that they terminated on either the twin boundaries or on the Shockley partial. This can be seen in Figs 1–3. (3) Lattice rotations were also observed, similar to those seen by Komoda (1968), as indicated in Fig. 1. These rotations were most noticeable along the surface, and were also present in particles which did not contain any dislocations. Moreover they cannot be accounted for by changes in particle thickness. Hence we conclude that the distortions in Ics are taken up by an inhomogeneous elastic strain in small Ics, and by a combination of dislocations and inhomogeneous elastic strains in larger particles. The defect structure is discussed in more detail in Section 4.1.

It is of relevance to consider the magnitude of the amplitude contrast associated with the defects in Ics. In small particles, no such strain contrast could be discerned whereas in slightly larger particles (e.g. Fig. 2), the contrast was visible, though small, and restricted to a narrow region near the fault. This low level of amplitude contrast is clearly not due to the exclusion of higher order diffracted beams in the lattice images, as evidenced by the BF-DF pair of STEM images shown in Fig. 3. In order to achieve this level of contrast in the BF image, it was neces-

rhombic form. Our previous high-resolution lattice imaging observations have shown little obvious evidence for inhomogeneous elastic strains, although demonstrating that small Ics contained a significant number of dislocations (Marks *et al.*, 1980; Smith & Marks, 1981a).

In this paper we report the results of a detailed study of defects and strains in MTPs employing a combination of high resolution lattice imaging and high resolution dark field as well as microdiffraction in a scanning transmission instrument. From the lattice fringe images we have been able to detect evidence for inhomogeneous elastic strains in the region of the surface of the Ics (Section 3.1), as well as details of the defect structure in the two types of MTPs (Sections 3.1 and 3.2). Both the inhomogeneous strains and the dislocations in the Ics produce mainly phase, rather than amplitude, contrast, an effect substantiated by the dark field images, and this explains why earlier lower-resolution work has failed to detect their presence. This interpretation of MTPs as inhomogeneously-strained and dislocated fcc aggregates is also substantiated by the microdiffraction results (Section 3.3). Collation of the experimental evidence allows models for the defects in both types of MTPs to be proposed (Section 4): the relative merits of the various techniques with respect to providing useful structural information is briefly discussed (Section 5).

2. EXPERIMENTAL PROCEDURE

The results presented below were obtained from a number of different samples—we report those generally consistent features which appeared to show little, or no, dependence upon preparation technique or the previous history of the sample.

The stock samples for Ics of gold and silver were prepared by evaporation in a diffusion-pumped system as described elsewhere (Marks & Smith, 1981). Somewhat larger MTPs (25–50 nm in diameter) were observed in a specimen evaporated onto a substrate of KCl, which had been cleaved *in situ* at 300°C in an unbaked, all-metal evaporator. (The primary nuclei in this specimen were (100) epitaxed square pyramids—MTPs were common only as secondary nuclei.) Very large Dhs were found in a silver catalyst sample, details of which have been published elsewhere (Marks & Howie, 1979). A somewhat different type of MTP was observed in a specimen of Au evaporated at room temperature on to *in situ* cleaved KCl in UHV ($< 2 \times 10^{-8}$ Pa). The Dhs in this sample were noticeably rounded (see Figs. 6 and 8), and contained a significantly larger number of defects. However, the actual defect structures appeared to be the same as those observed in particles prepared by other means.

The high resolution lattice images of MTPs were taken with the Cambridge University High Resolution Electron Microscope (HREM) (Smith *et al.*, 1982) operated at either 500 kV or 575 kV. Initially, micrographs from areas of interest were recorded as through focal series (Marks & Smith, 1981) but recent work has been carried out using an image pickup system (Catto *et al.*, 1982). The lattice structure of the particles could then be directly viewed on the television monitor and the required defocus could be chosen with considerable accuracy.

For STEM imaging, and microdiffraction mappings, specimens were examined in a VG-HB5 electron microscope operated at 80 kV. As a compromise between resolution and signal strength, a large objective aperture ($\sim 0.2 \text{ \AA}^{-1}$ radius) and a relatively small collector aperture ($\sim 1\frac{1}{2}$ mrad radius) were normally used, with the condenser lens overexcited to reduce the effects of stray fields in the region of the gun. (The visibility of the 6.8 Å Moire fringes in MTPs was used as a resolution check.) The microdiffraction maps were collected with a Grigson scanning system, with some low pass filtering to minimize the effects of instrument noise and amorphous carbon speckle structure.

3. EXPERIMENTAL RESULTS

3.1. Icosahedral MTPs

The basic defect structure observed in the icosahedral particles is shown in Fig. 1; namely, a stacking fault which lies parallel with the external surface terminating on a Shockley partial dislocation and extending part-way across one of the (110) oriented segments. The length of the stacking fault and the total number of defects per particle varied somewhat, but a number of

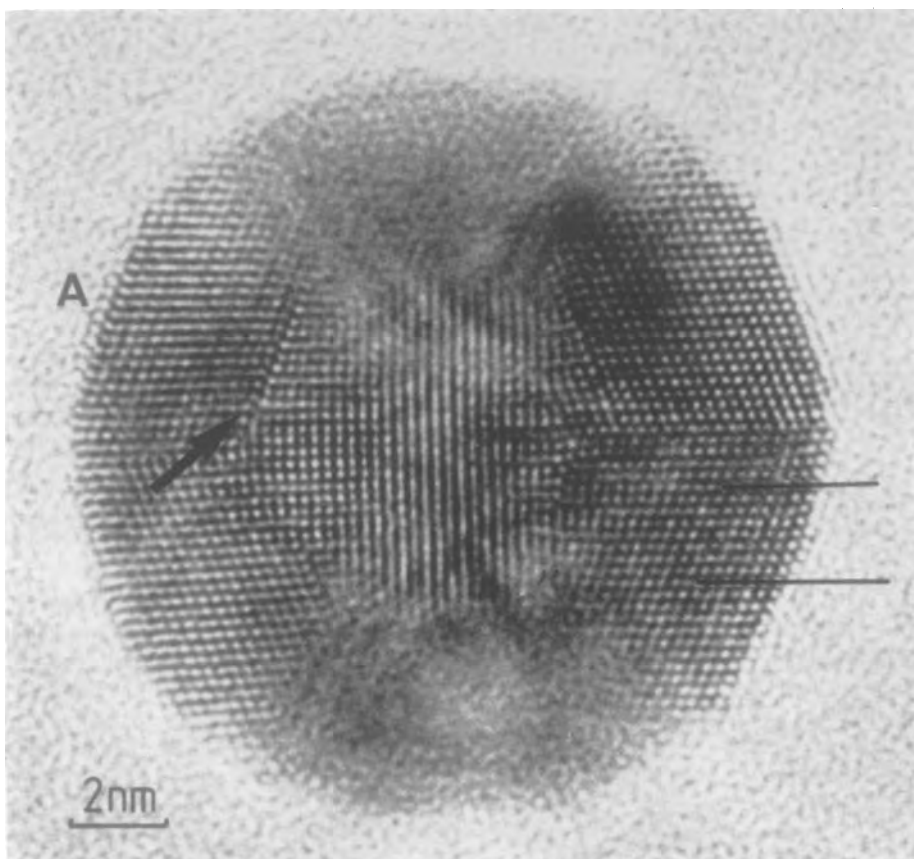


Fig. 1. High resolution lattice image of an Ic showing the basic defect structure. The Shockley partial dislocation and some lattice rotations are indicated. A partial layer where an ordering mistake has occurred can be seen at A.

general characteristics were observed: (1) The defects were present only in particles above about 15 nm in diameter, and showed a noticeable increase both in the number of defects per particle, and the length of the stacking fault, with increasing particle size. An example of a particle containing three dislocations in one segment is shown in Fig. 2. (2) The stacking faults never showed any evidence for reflection across the twin boundaries indicating that they terminated on either the twin boundaries or on the Shockley partial. This can be seen in Figs 1–3. (3) Lattice rotations were also observed, similar to those seen by Komoda (1968), as indicated in Fig. 1. These rotations were most noticeable along the surface, and were also present in particles which did not contain any dislocations. Moreover they cannot be accounted for by changes in particle thickness. Hence we conclude that the distortions in Ics are taken up by an inhomogeneous elastic strain in small Ics, and by a combination of dislocations and inhomogeneous elastic strains in larger particles. The defect structure is discussed in more detail in Section 4.1.

It is of relevance to consider the magnitude of the amplitude contrast associated with the defects in Ics. In small particles, no such strain contrast could be discerned whereas in slightly larger particles (e.g. Fig. 2), the contrast was visible, though small, and restricted to a narrow region near the fault. This low level of amplitude contrast is clearly not due to the exclusion of higher order diffracted beams in the lattice images, as evidenced by the BF-DF pair of STEM images shown in Fig. 3. In order to achieve this level of contrast in the BF image, it was neces-

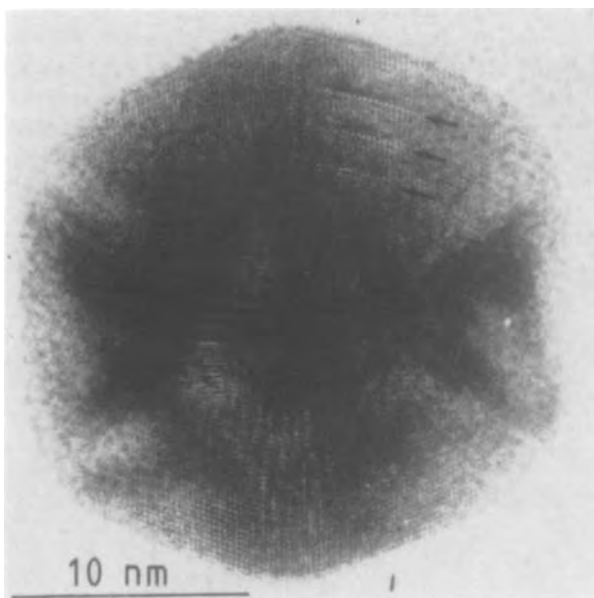


Fig. 2. High resolution lattice image of an Ic showing three defects (arrowed).

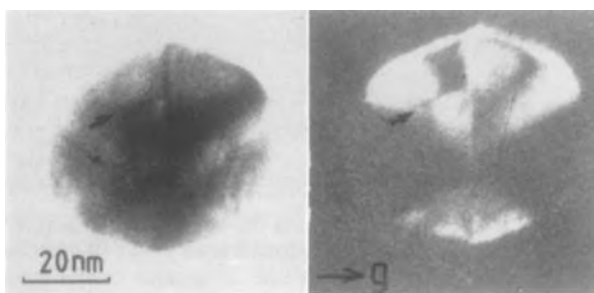


Fig. 3. A STEM BF-DF pair taken with the g vector shown: the defect line is arrowed.

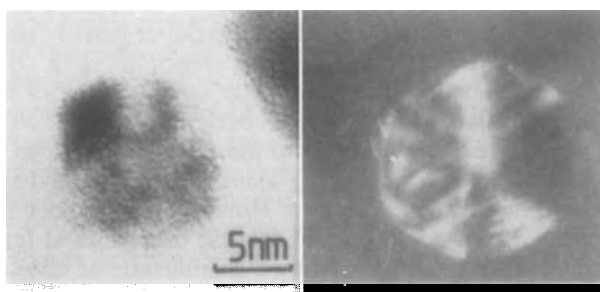


Fig. 4. A BF-DF amplitude contrast pair taken at 500 kV. Due to overlap of various diffracted beams in the image, it is not possible to decide if any defects are present.

sary to employ extreme conditions, electronically enhancing the particle contrast such that the image of the amorphous carbon background became heavily saturated resulting in the loss of other useful information such as the external profile. Even then, the defect (arrowed) is only just discernible. In the dark field image the presence of the defect is clearer, although it should

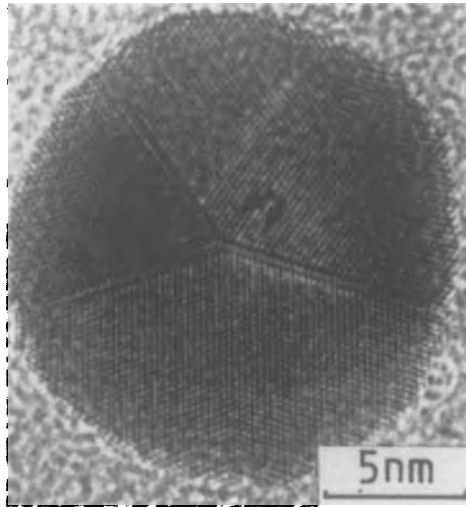


Fig. 5. High resolution lattice image of a Dh, with strong contrast variations in the (111) fringes arrowed.

be pointed out that this image was unusual. It was much more common, particularly with smaller particles, as in Fig. 4, that no positive identification was possible from the DF images because of confusion arising from extinction contours and overlapping segments.

It is relevant here to note a major limitation in the use of DF techniques in the characterization of small particles which is the uncertainty in their orientation. It is our experience that there is usually considerable variation in local orientation (the 10° difference for the decahedra of Figs. 11 and 12 perhaps represents an extreme case). Moreover, keeping track of a single particle amongst the typical 10^6 particles in a grid square whilst changing specimen tilt is not easy. This makes quantitative weak-beam techniques very difficult to use.

3.2. Decahedral MTPs

With the decahedral particles, defects were localized to regions near the twin boundaries. Evidence for two effects was observed, namely twin boundary relaxations and stacking faults running parallel with, and near to, the boundaries.

With small particles, no obvious lattice fringe rotations were observed in the bulk of the particles which could be reliably interpreted as due to an inhomogeneous strain, as reported previously (Marks & Smith, 1981), although marked variations due to extinction contours were clearly observed. In many particles, noticeable contrast variations were observed near the twin boundaries and strong intensity variations were frequently seen in the (111) fringes running parallel with these boundaries, as illustrated in Fig. 5. Alternatively, the appearance of the fringes suggested a small shear and a small gap at the twin boundaries as shown in Fig. 6. Contrast variations such as lattice shifts and gaps are imaging effects which occur when twin boundary relaxations are present (G. J. Wood, private communication), although it should be pointed out that images with similar appearances could result from astigmatism or misalignment *should* these be present. Unfortunately, insufficient quantitative information is currently available concerning the contrast effects in lattice images associated with twin boundary relaxations (e.g. Wood *et al.*, 1982) so that these effects cannot be properly quantified.

In larger particles (in general, 30 nm in diameter or more), there was a loss of the five-fold rotational symmetry, and stacking faults occurred near the twin boundaries. No obvious defect structure with dislocations were seen, but a number of other general observations could be made: (1) In many cases, one or more of the twin boundaries had migrated, so that all five segments no longer met—an example of this is shown in Fig. 7. (2) A series of stacking faults often ran parallel with, and adjacent to, the twin boundaries—an example is shown in Fig. 8.

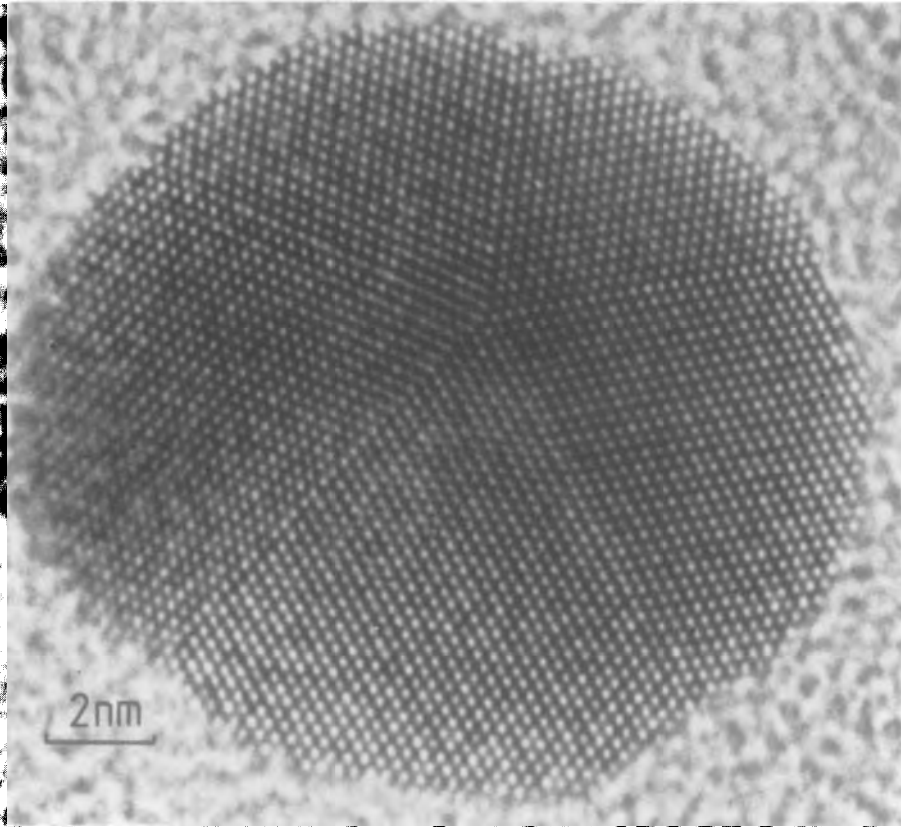


Fig. 6. High resolution image of a Dh (from the room temperature sample) where shears and gaps in the fringe structure are evident at the twin boundaries.

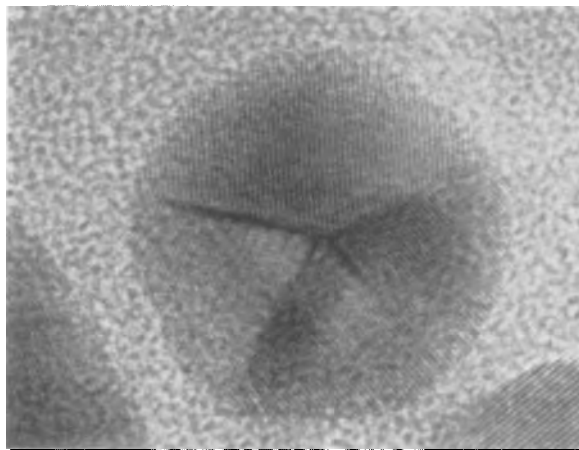


Fig. 7. Lattice image of a small Dh showing a mismatch between two of the segments which are separated by 4.7 Å.

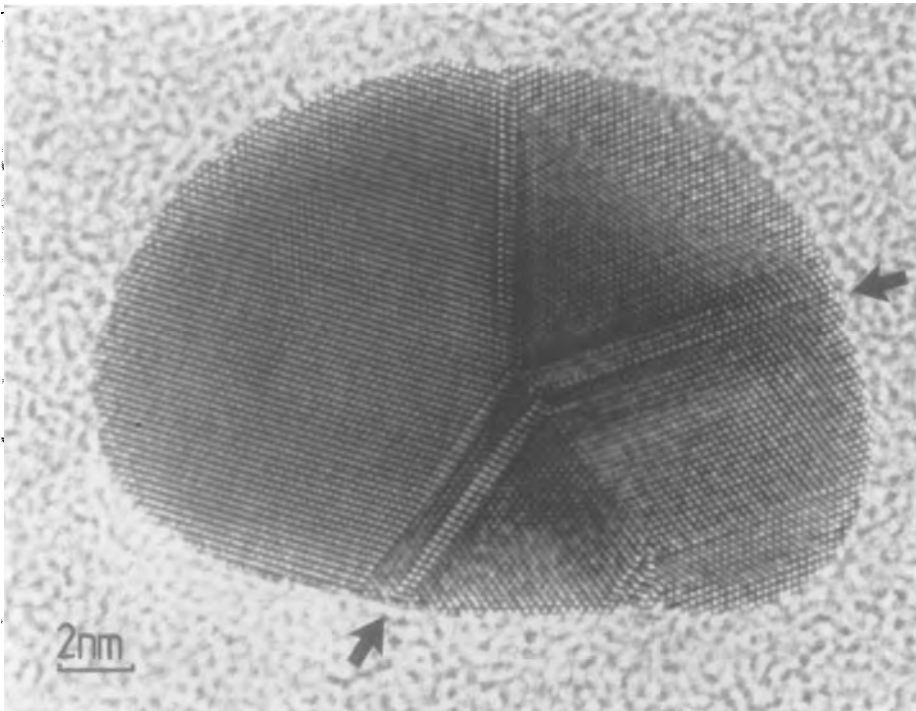


Fig. 8. Micrograph of a Dh (from the room temperature sample) with stacking faults running across the particle as arrowed.

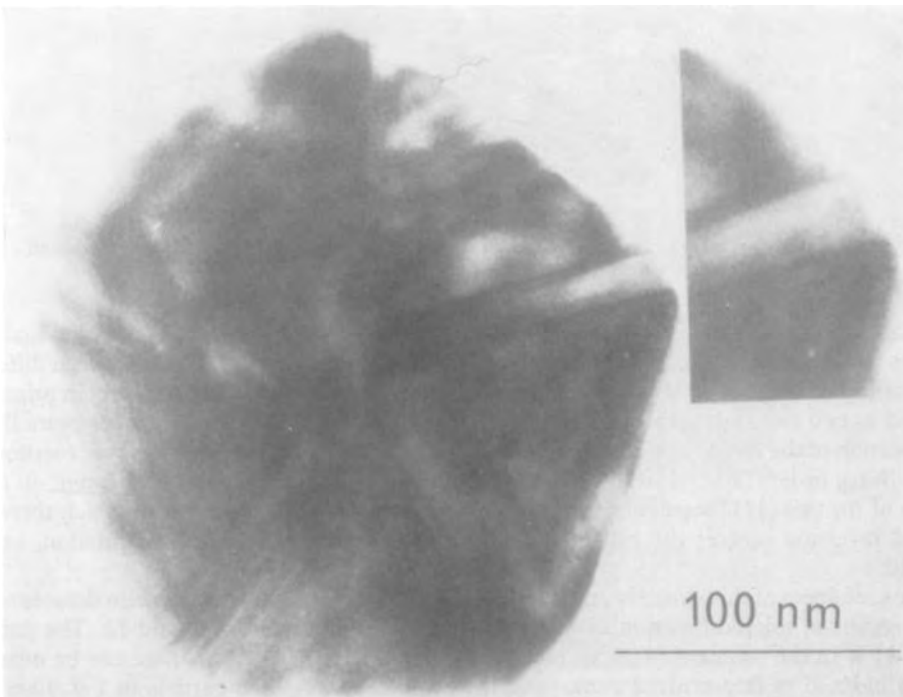


Fig. 9. Bright field amplitude contrast image of a Dh which shows evidence for migration of the twin boundaries, stacking faults and extrusion of material (see inset area).

Similarly details in large particles have previously been published by Marks & Howie (1979). (3) There was extrusion of material near these stacking faults, particularly in larger particles (e.g. in Marks & Howie, 1979)—see Fig. 9.

3.3. *Microdiffraction maps*

Microdiffraction mapping provides diffraction information concerning spacings well below the resolution limit of a lattice image. This is particularly useful with MTPs where only a few of the segments may be oriented to excite the low order beams used in lattice imaging. The microdiffraction mapping of an Ic, shown in Fig. 10, illustrates the extensive information

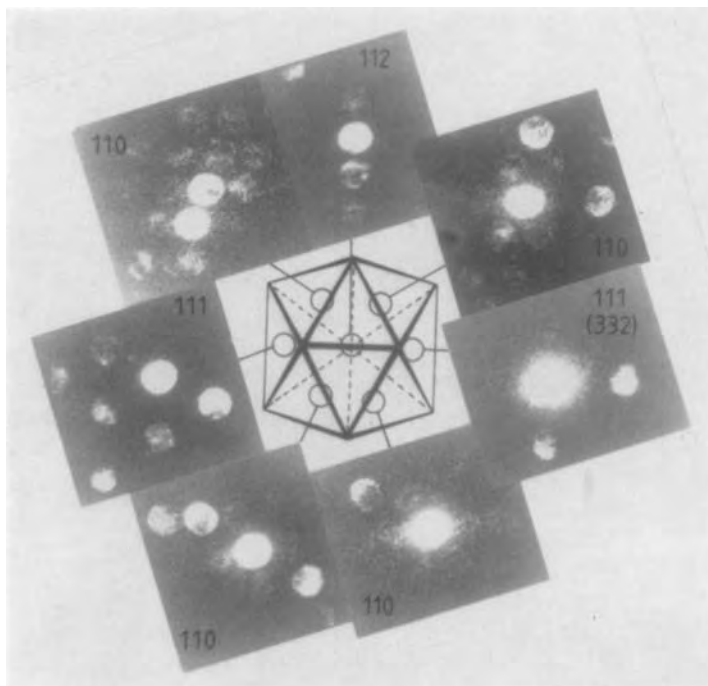


Fig. 10. Microdiffraction map from Ic of 30 nm diameter with probe locations as indicated.

available. An immediate conclusion from the results is that the structure of the individual segments is face-centred cubic. A second feature is the marked lack of symmetry between different parts of the particle. For instance, there are four (110) oriented segments which are, in principle, arranged as two twin-related pairs, with the twin boundary normal to the incident beam direction: location of the Ewald spheres using the strongly diffracting spots indicates that rotations of several Bragg orders (several degrees) are present. An even larger rotation is apparent on comparison of the two (111) segments on the left and right of the particle between which there is a nominal inversion centre: the right-hand segment has rotated to a (322) orientation, i.e. by about 10° .

The usefulness of this extensive information concerning the orientations is also demonstrated by the results of microdiffraction mappings of Dh's, as shown in Figs. 11 and 12. The particle in Fig. 11 is in the standard (111) epitaxial orientation, and the patterns here can be unambiguously indexed as face-centred cubic (and not orthorhombic). The particle in Fig. 12 is also face-centred cubic in structure, but the lower 'epitaxial' segment here has a (332) orientation relative to the electron beam which is about 10° from a (111) orientation. Differentiation between

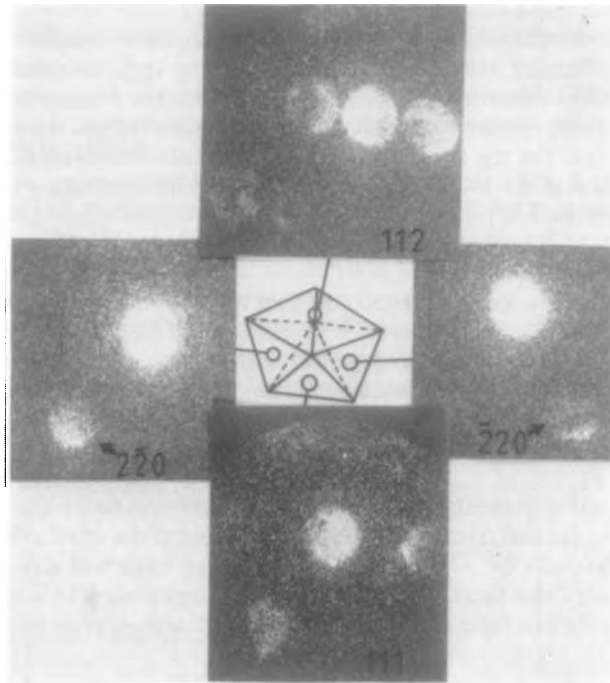


Fig. 11. Microdiffraction map of a 30 nm diameter Dh in the $\langle 111 \rangle$ epitaxial orientation. The locations of the probe are indicated on the Figure.

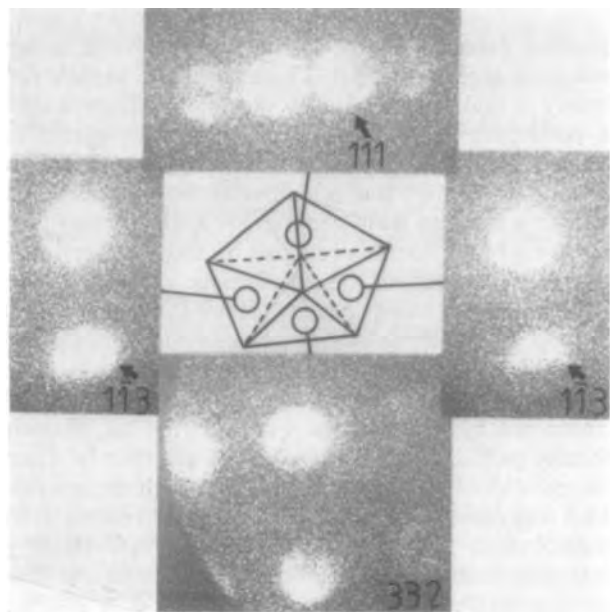


Fig. 12. Microdiffraction map from a 30 nm diameter Dh where the 'epitaxial' segment has rotated by about 10° to a (332) orientation.

the two orientations in Figs. 11 and 12 by microdiffraction is straightforward, but would be very time-consuming, if not impossible, by any other technique.

The two different orientations of these particles, despite their separation by only ~ 30 nm, were indicative of a difficulty with Dh's associated with their apparent local epitaxy. Examinations by HREM confirm variations in orientation about the arc defined by the (111) epitaxial orientations and the (110) symmetry orientation—(111) lattice fringes were always observed in two of the segments (i.e. the top two in Fig. 11). These observations correlate with the effects reported by Heinemann *et al.* (1979) which were, however, interpreted by these authors as due to a change in the structure.

4. DEFECT MODELS

In this section, specific models are described for the defect structures observed experimentally. However, because of the implicit ambiguities resulting from imprecise knowledge of the local diffraction conditions and confusion from overlapping tetrahedra, our analysis is admittedly qualitative but correlates well with isotropic inhomogeneous elasticity solutions for MTPs which are developed in detail elsewhere (Howie *et al.*, 1983).

4.1. Icosahedral MTPs

The type of distortion present in Ics (assuming perfect symmetry and no defects) can be considered as applying normal tractions to the twinned faces of the tetrahedral units, expanding the angle between the faces by $\sim 1\frac{1}{2}^\circ$ to 72° . (A balancing force will also be required on the vertex common to these three faces.) Approximating the outer surface by a sphere and assuming rotational symmetry, the isotropic stress field can be summarized, after Howie *et al.* (1983):

$$\begin{aligned}\sigma_{rr} &= \frac{\Delta\Omega}{4\pi} \cdot \frac{2\mu(1+\nu)}{3(1-\nu)} \ln(r/R) \\ \sigma_{\theta\theta} = \sigma_{\phi\phi} = \sigma_{rr} + \frac{\Delta\Omega}{4\pi} \cdot \frac{\mu(1+\nu)}{3(1-\nu)} \\ \sigma_{r\theta} = \sigma_{\theta\phi} = \sigma_{\phi r} &= 0\end{aligned}$$

where r , θ , ϕ are spherical polar co-ordinates, ν is Poisson's ratio, μ is the shear modulus, $\Delta\Omega/4\pi$ is the fractional solid angle deficit = 0.123, and R is the particle radius. To relieve this stress field, it is necessary to find a mechanism to expand the effective solid angle of the tetrahedron. Three main possibilities exist: (a) glide of a Shockley partial in from the surface; (b) climb of a Frank partial from the surface; (c) a mixture of climb and glide of a full dislocation. Alternatives (a) and (c) can be ruled out directly from the experimental micrographs: there was no evidence for a stacking fault running out to the surface as required by (a), nor was there any evidence for a full dislocation or a pair of Shockley partials. For mechanism (b), the most favourable direction for climb will be radially since $\sigma_{\theta\theta} > \sigma_{rr}$, and along a twin boundary where there would be no additional energy penalty arising from stacking fault formation. However, a Frank partial loop cannot climb completely into the centre of the particle since $\sigma_{\theta\theta}$ changes sign: it will stop near to a value of r corresponding to $\sigma_{\theta\theta} = 0$, i.e. $r = 0.607R$. (This penetration distance is in reasonable agreement with the experimental results.)

A further mechanism will now occur: the Frank partial can dissociate into a stair-rod dislocation and a Shockley partial. The Shockley partial will then be driven to glide part way across the tetrahedron, parallel to the external surface, by both the inter-dislocation repulsion, and shear stresses. (Part way only, since the shear stresses will reverse in sign if the dislocation goes past the plane normal to the Burgers vector and running through the particle centre. This plane lies well inside the tetrahedron.) This defect structure, which is illustrated in Fig. 13, is consistent with the experimentally-observed defects.

4.2. Decahedral MTPs

The defect structure observed in the Dh's is not a 'standard' dislocation formation but one

which can be directly related to the overall defect geometry of these particles. Dh's are a well-known example of a disclination (a common name for the Dh structure is a star disclination), which is a rotational defect in contrast to dislocations which are translational defects. There is a two-dimensional angular deficit of $\sim 7\frac{1}{2}^\circ$ when the particles are constructed from five twin-related segments, which can be eliminated by an inhomogeneous strain. (The strain field for this type of defect dates back to the original dislocation analysis by Volterra; a solution was given more recently by de Wit (1972).)

A property of a 'wedge' or screw disclination, such as exists in a Dh, is that an edge dislocation can terminate on the disclination (see deWit, 1969). From the analysis of de Wit (1969), it is clear that running a Shockley or Frank partial along the twin boundary of a Dh migrates the disclination by one atomic spacing normal to the twin boundary. This effect is illustrated in Fig. 14. The resultant configuration corresponds to a new location of the disclination at C rather than O, and a vacancy region in OBC. Assuming a Frank partial as in Fig. 14, and a migration of the stacking fault, then this configuration corresponds to the experimental micrograph of Fig. 7. The various different experimental features correspond to alternatives of the same basic result of disclination migration.

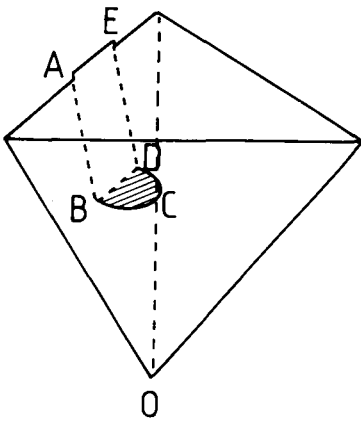


Fig. 13

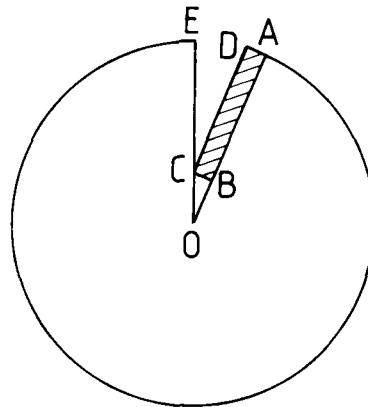


Fig. 14

Fig. 13. Diagram for the proposed defect structure in icosahedral MTPs. One tetrahedral segment is shown, with O denoting the centre of the particle and AE points lying on the surface. The shaded stacking fault bounded by BCD corresponds to the experimentally observed defect, the line BCD being a Shockley partial, BD a stair-rod dislocation with AB and DE corresponding to Frank dislocations at the twin boundary.

Fig. 14. Diagram to illustrate the relationship between an edge dislocation, a wedge disclination and the proposed defect structure (A wedge disclination is an angular defect, such as the gap AOE, which is $7\frac{1}{2}^\circ$ in a Dh.) Introduction of extra material (ABCD) into the defect migrates the twin boundary from AB to CD and may leave behind a residual stacking fault along AB. The disclination moves from O to C, and a small vacancy region is left in OBC.

5. DISCUSSION

On the basis of the different types of information that HREM and STEM provide about MTPs, it seems appropriate to discuss briefly the relative merits of these instruments for characterizing small particles (see also Howie *et al.*, 1982). In several respects it is clear that the information available overlaps. The power of HREM lattice imaging lies in its high spatial resolution which provides highly localized information about the diffraction conditions. However, at least for metallic crystals, details are limited to the low order diffracted beams. By way of comparison, STEM microdiffraction provides high resolution detail on the diffraction

conditions but has a comparatively limited spatial resolution. Overlap occurs when the experimental conditions are not too demanding for both image and diffraction space information. For example, both lattice imaging (e.g. Smith *et al.*, 1981) and STEM microdiffraction (e.g. Pennycook, 1981) are capable of indexing the crystallographies of metal particles.

In other areas, the methods do not really overlap, but are complementary. High resolution lattice imaging is a more powerful technique for decoding particle structures (see, for example, Smith & Marks, 1981b), and obtaining local information such as the defect structures described herein. STEM microdiffraction is more useful in obtaining information about local orientation information, with an accuracy of about 1° , as evidenced in Section 3.3. The two techniques complement each other when they combine to remove ambiguities in a physical problem, as in the identification of an inhomogeneously-strained fcc structure for MTPs.

When the two types of instrument are employed for more conventional studies, such as diffraction contrast BF-DF imaging, there is more competition in their relative merits. In the HREM there is no problem with instrument noise in a diffraction contrast mode, but it is often necessary to record micrographs 'blind' due to the present unavailability of adequate image intensification devices; for example, the DF micrograph in Fig. 4 was recorded on the off-chance that it might show some form of obvious dislocation contrast, but without success. By comparison, the BF-DF pair in Fig. 3 was visible on the screen, and it was possible to locate the defect. This illustrates the benefits provided by electronic signal detection in a STEM since this allows the contrast levels to be improved markedly, as shown in Section 3.1. Furthermore, micro-diffraction patterns from defected segments makes it very simple to set up the DF conditions.

Unfortunately, instrumental noise places a severe limitation on the power of the STEM DF techniques. In practice, weak beam conditions were not really accessible in a STEM, although readily available in the HREM but with no reliable information about the diffraction conditions. Weak beam techniques have been used in previous observations of small particles, as shown in the review by Heinemann *et al.* (1980).

Finally, there are some areas where the two instruments provide totally different information with no appreciable overlap. For example, the ability of the STEM to collect many different types of signal can be gainfully exploited. Chemical information can be collected from a single particle, as demonstrated by Pennycook (1981). Alternatively, the different signals can be employed in a 'Z contrast' mode to show clearly single atoms (Crewe *et al.*, 1975) or small catalyst particles (Treacy *et al.*, 1978). The interaction between an electron probe and the electrons near to a surface can also be investigated by imaging the low energy surface plasmon losses (Cowley, 1982; Marks, 1982).

An area where the HREM seems unique at present is in its capability to image directly the particle surface. For example, following recent improvements to the 600 kV HREM, continuous contrast transfer is now being obtained down to about 1.8 \AA (Smith *et al.*, 1983) and, under these conditions, phase contrast effects due to surface structure can be discerned in the images. Surface structure and surface steps are clearly seen in the particles shown in Figs. 1, 5, 6 and 8. The usefulness of these images is exemplified by the ordering mistake on the surface of the Ic seen in Fig. 1. A more detailed description of this direct surface imaging will be given elsewhere.

In conclusion, the choice of a STEM or an HREM instrument for the study of small particles depends upon what information is being sought. In some respects the instruments overlap; in others, totally different information is provided. In some cases, such as with MTPs, they provide a powerful combination.

ACKNOWLEDGMENTS

We are indebted to Drs A. Howie, E. Yoffe and L. M. Brown for advice and discussion, particularly relating to the defect models, and acknowledge support from the Science and Engineering Research Council.

REFERENCES

- Allpress, J.G. & Sanders, J.V. (1967) Structure and orientation of crystals in deposits of metals on mica. *Surf. Sci.* **7**, 1.
- Catto, C.J.D., Smith, K.C.A., Nixon, W.C., Erasmus, S.J. & Smith, D.J. (1982) An image pickup and display system for the Cambridge University HREM. In: *Electron Microscopy and Analysis*, 1981 (Ed. by M. J. Goringe), pp. 123–126. Institute of Physics, Bristol and London.
- Cowley, J.M. (1982) Energy losses of fast electrons at crystal surfaces. *Phys. Rev. B*, **25**, 1401.
- Crewe, A.V., Langmore, J.P. & Isaacson, M.S. (1975) Resolution and contrast in the STEM. In: *Physical Aspects of Electron Microscopy and Microbeam Analysis* (Ed. by B. M. Siegel and P. R. Beaman), pp. 47–62. Wiley, New York.
- Heinemann, K., Avalos-Borja, M., Poppa, H. & Yacaman, M.J. (1980) The characterisation of small metal particles by selected-zone dark field and weak-beam dark field TEM. In: *Electron Microscopy and Analysis*, 1979 (Ed. by T. Mulvey), pp. 387–392. Institute of Physics, Bristol and London.
- Heinemann, K., Yacaman, M.J., Yang, C.Y. & Poppa, H. (1979) The structure of small, vapour-deposited particles. I. Experimental study of single crystals and particles with pentagonal profiles. *J. Crystal Growth*, **47**, 177.
- Howie, A., Marks, L.D. & Pennycook, S.J. (1982) New imaging methods for catalyst particles. *Ultramicroscopy*, **8**, 163.
- Howie, A., Marks, L.D. & Yoffe, E. (1983) In preparation.
- Ino, S. (1966) Epitaxial growth on rocksalt faces cleaved in vacuum. 2. Orientation and structure of gold particles formed in ultrahigh vacuum. *J. Phys. Soc. Japan*, **21**, 346.
- Ino, S. & Ogawa, S. (1967) Multiply-twinned particles at earlier stages of gold film formation on alkali halide crystals. *J. Phys. Soc. Japan*, **22**, 1365.
- Komoda, T. (1968) Study on structure of evaporated gold particles by means of a high resolution electron microscope. *Jap. J. appl. Phys.* **7**, 27.
- Marks, L.D. (1982) Observation of the Image Force for fast electrons near an MgO surface. *Sol. State Comms*, **43**, 727.
- Marks, L.D. (1983) Surface structure and energies of multiply twinned particles. *Phil. Mag.* (in press).
- Marks, L.D. & Howie, A. (1979) Multiply-twinned particles in silver catalysts. *Nature*, **282**, 196.
- Marks, L.D., Howie, A. & Smith, D.J. (1980) In: *Electron Microscopy and Analysis* 1979 (Ed. by T. Mulvey), pp. 397–400. Institute of Physics, Bristol and London.
- Marks, L.D. & Smith, D.J. (1981) High resolution studies of small particles of gold and silver. I. Multiply-twinned particles. *J. Cryst. Growth*, **54**, 425.
- Pennycook, S.J. (1981) Study of supported ruthenium catalysts by STEM. *J. Microsc.* **124**, 15.
- Smith, D.J., Fisher, R.M. & Freeman, L.A. (1981) High-resolution electron microscopy of metal-intercalated 'Graphimets'. *J. Catal.* **72**, 51.
- Smith, D.J. & Marks, L.D. (1981a) Direct lattice imaging of small metal particles. *Phil. Mag. A*, **44**, 735.
- Smith, D.J. & Marks, L.D. (1981b) High-resolution studies of small particles of gold and silver. II. Single crystals, lamellar twins and polyparticles. *J. Cryst. Growth*, **54**, 433.
- Smith, D.J., Camps, R.A., Cosslett, V.E., Freeman, L.A., Saxton, W.O., Nixon, W.C., Ahmed, H., Catto, C.J.D., Cleaver, J.R.A., Smith, K.C.A. & Timbs, A.E. (1982) Optimisation and applications of the Cambridge University 600 kV High Resolution Electron Microscope. *Ultramicroscopy*, **9**, 203.
- Smith, D.J., Camps, R.A., Freeman, L.A., Hill, R., Nixon, W.C. & Smith, K.C.A. (1983) Recent improvements to the Cambridge University 600 kV High Resolution Electron Microscope. *J. Microsc.* **130**, 127.
- Treacy, M.M.J., Howie, A. & Wilson, C.J.Z. (1978) Z contrast of platinum and palladium catalysts. *Phil. Mag. A*, **38**, 569.
- Wit, R. de (1969) In: *Fundamental Aspects of Dislocation Theory* (Ed. by J. A. Simmons, R. de Wit and R. Bulbough), Vol. 1, p. 651 and, in particular, pp. 677–680. Nat. Bur. Stand (U.S.) Spec. Publ. 317, Vol. 1.
- Wit, R. de (1972) Partial disclinations. *J. Phys. C*, **5**, 529.
- Wood, G.J., Stobbs, W.M. & Smith, D.J. (1982) On Fresnel diffraction and twin boundary displacements in copper. In: *Electron Microscopy* 1982, Vol. 2, p. 341.
- Yacaman, M.J., Heinemann, K., Yang, C.Y. & Poppa, H. (1979) The structure of small, vapour-deposited particles. II. Experimental study of particles with hexagonal profile. *J. Crystal Growth*, **47**, 187.
- Yang, C.Y. (1979) Crystallography of decahedral and icosahedral particles. I. Geometry of twinning. *J. Crystal Growth*, **47**, 274.
- Yang, C.Y., Yacaman, M.H. & Heinemann, K. (1979) Crystallography of decahedral and icosahedral particles. II. High symmetry orientations. *J. Crystal Growth*, **47**, 283.